Journal of Sound and Vibration (1997) **199**(4), 645–666

A SEA-LIKE APPROACH FOR THE DERIVATION OF ENERGY FLOW COEFFICIENTS WITH A FINITE ELEMENT MODEL

C. R. FREDÖ

Department of Applied Acoustics, Chalmers University of Technology, S-412 96 Gothenburg, Sweden

(*Received* 26 *June* 1993, *and in final form* 3 *June* 1996)

The Finite Element method is combined with a Statistical Energy Analysis-like (SEAL) energy flow balance to derive the power transmission between two thin plates. A fundamental difference between SEA and the SEAL procedure is that the former is applied to ensembles, while the latter addresses the individual case. Energy Flow Coefficients (EFCs) are derived and explicit use of the non-resonant part of the kinetic energy is made. It is demonstrated that the EFC, as opposed to the SEA Coupling Loss Factor (CLF), can become negative at some frequencies. The EFC exhibits characteristics that are individual for each case examined, although it tends towards the CLF at high frequencies. It is also shown that the SEAL energy flow balance can be used for narrow bands, and at any frequency.

1. INTRODUCTION

Energy flow methods such as Statistical Energy Analysis (SEA) [1] and the Statistical Energy Method (SEM) [2] are today widely used and there are numerous examples of successful applications. SEA and SEM are used predominantly at high frequency: i.e., at frequencies at which the subsystem size is large in comparison with the wavelength. Basic to these techniques is that the energy flow within a system can be related to the difference in vibrational energy between parts of the system. Various types of energy transmission factors that can be used to describe the size of this energy flow exist; notable among them are the Coupling Loss Factor, the Energy Conductance and the Transmission Factor, as defined in references [1–3], respectively. However, a strict experimental derivation of these factors can be difficult, owing to conditions intrinsic in their definition: e.g., that they relate to systems of infinite size [3] or that they apply for ensembles [1, 2]. The applicability of the factors in predicting the flow of energy in an individual engineering structure can also be limited, especially at low frequency, as the assumptions on which they are based break down. Therefore, alternative approaches that do not suffer from such limitations are of interest.

Traditional use of the Finite Element (FE) method for dynamic analysis of mechanical structures is typically found for low frequencies with only a few modes included in the analysis. Restrictions in the use of the FE method are often imposed by computational expense for analysis at high frequencies, where a dense FE mesh is necessary to resolve the response and where the high frequency limit is dependent on the system's size and complexity. On the other hand, SEA is restricted: (i) to high frequency applications, as assumptions concerning uniformity of the energy density in the response field break down

0022–460X/97/040645 + 22 $25.00/0/sv960634

at low frequency; (ii) from lack of appropriate coupling data, and sometimes also because the source spectrum is not suitable, e.g., is concentrated to narrow bands or has sharp peaks. Both the FE and SEA methods have been successfully applied to various tasks; however, several engineering problems do not clearly fall within the individual method's domain of application. Creating a deterministic model for some parts of the structure and combining it with a statistical model for the other parts is thus appealing. Coupling factors can be generated for parts of the energy flow model that are not amenable to traditional analysis or for the purpose of analyzing regions where SEA provides a poor estimate. In the above mentioned approach, detailed analysis is carried out only for some regions of the system, which consequently allows the FE analysis to be applied for higher frequencies for the investigated parts than for the complete system.

The focus here is on examining the use of an energy flow balance for the individual case, exploiting the philosophy and formalism in SEA rather than applying its underlying assumptions and rules in the process of analysis. Differences between this approach and SEA are emphasized in order to demonstrate assumptions that can be used for the ensemble but not for the single specimen, as the individual case normally differs from the mean in an ensemble of cases. Clarifying such diversities can be seen as a step toward the above mentioned combined use of SEA and the FE method. This paper addresses the issue of how the deterministic part of such a model can be treated with the FE method.

Use of the FE method in generating coupling data is appealing because of its versatility when applied to systems of finite size, which was foreseen by Lyon in reference [1]. Combining the SEA philosophy with results from FE computations offers more of a "D'Alembertian approach" to the derivation of energy flow than do intensity or mobility methods, in the sense that detailed information about the interaction between subsystems is not explicitly used. Post-processing the FE-computed data is simple when scalar quantities such as power and subsystem energies are used, as they do not require explicit information concerning the co-ordinate system.

Use of the FE method for determining the energy flow is not new, however, and several approaches have been used: e.g., Power Flow Finite Elements (PFFEM) [4–6], FE-computed transmission coefficients [7, 8], mobility power flow [9] and structural intensity [10, 11]. In the PFFEM approach in references [4–6] the coupling data is used as input to the analysis and thus cannot be used for deriving the coupling factors. In the approaches in references [7, 8] the FE method is used to derive transmission factors in a way similar to the traditional wave analysis in reference [3]. The concept of computing the transmission coefficient is appealing and allows the output to be used in SEA, although the approach seems to have been applied for beam structures only. The approaches in references [9–11] are based on intensity or mobility, i.e., vector information in which the spatial derivatives of the displacement are used (e.g., transverse force and moment). A less dense mesh and fewer modes in the modal summation better suffice for the current approach than for the mobility or structural intensity approaches, as it only involves use of displacements, (and rotations), and not its higher derivatives. Higher derivatives require a more precise FE model to converge to the same accuracy as the displacements, as was shown in reference [10]. An elegant means to reduce the error from modal truncation by use of the static solution in the computation of structural intensity was also presented in reference [10] for the case of point excitation. A modal basis produces results that converge for the complete system, but not necessarily for the local point, and thus subsystem energy is likely to be less affected by use of the modal basis than are mobility or structural intensity. Derivation of FE-computed coupling factors with SEAL approaches can be found in, e.g., references [12–14]. Approaches in which analytical models have been used to test SEA also exist; see, e.g., references [15–20].

Energy flow is derived in this presentation with a commercial FE code for a thin L-shaped plate and an example is presented of the possibility for using an energy flow model at low frequency. The FE model is validated for two separate cases. Measurements are used for the case of point excitation and free-free boundaries. An analytical model [12, 15, 16], based on thin plate theory, is used for comparison with the case of rain-on-the-roof excitation and simply supported boundaries.

2. THE FINITE ELEMENT MODEL

The example consists of two rectangular Perspex plates. Figure 1(a) shows the FE realization of the plates, dimensioned to have at least three elements per free bending wavelength, i.e., seven nodes per wavelength [21, 22], and with 189 eight node quadrilateral shell elements (S8R) with six degrees of freedom per node and the aspect ratio 1·1. This criterion gives an upper frequency limit for the FE mesh of approximately 1350 Hz and a total size of 3816 d.o.f. for the FE model, solved by using ABAQUS Version 4.9.

The experimental set-up and a measurement position are shown in Figure 1(b). Rain-on-the-roof excitation and simply supported boundary conditions are difficult to achieve in practice and thus experimental verification of the FE model is instead performed for point excitation with free-free boundary conditions. The L-plate was suspended from the ceiling by thin strings to approximate the free-free boundary conditions, and the rotational acceleration on both sides of the joint was measured and compared to ensure that the (glued) joint was sufficiently rigid in the frequency range considered. The force transducer was positioned directly on the exciter to reduce the loading of its rotational inertia on the measurement object as it was found to be significant for frequencies above 400 Hz. The stinger was designed according to reference [23] to avoid stinger rod resonances in the measured frequency range. Point mobilities were measured, and the critical damping ratio per mode was derived with circle-fitting and found to vary between 3% at low frequency and 1% at high frequency. For simplicity, a critical damping ratio of 2% is used for all modes in the following analysis.

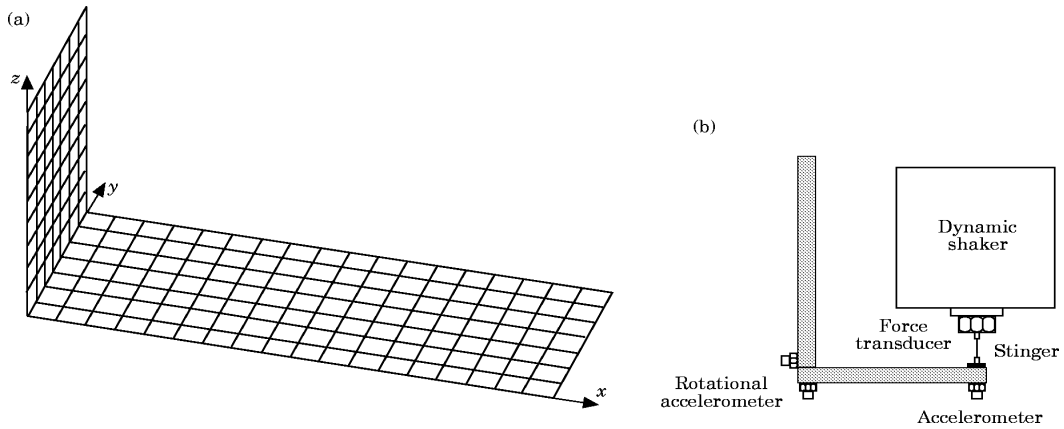

Figure 1. The investigated L-shaped plate. Dimensions are as follows: lengths, 0·39 m for the junction, 0·5 m for the smaller plate, 1·0 m for the larger plate; the thickness is 0·01 m for both plates. Material data are Young's modulus $4{\cdot}9 \times 10^9$ N/m^2, Poisson ratio 0·25, density 1180 kg/m^3. For the critical damping ratio, ζ, 2×10^{-2} was used as the modal damping factor. (b) The measurement set-up. The signals were processed with a GenRad 2515 FFT analyzer. Other measurement equipment used was force transducer B&K 8200, accelerometer B&K 4393, rotational accelerometer, Kistler Translational-Angular Transducer 8832 TAP system, charge amplifier B&K 2635, and B&K mini-shaker 4810.

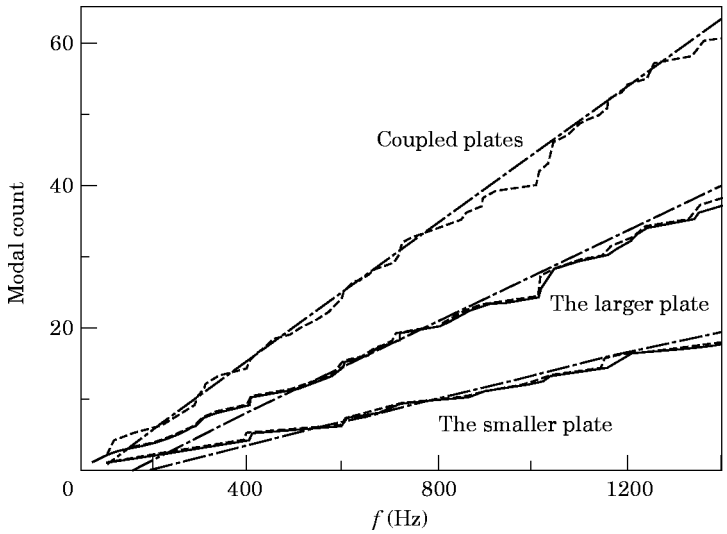

Figure 2. The number of eigenfrequencies for the simply supported case: ——, uncoupled plates, analytical model; – –, FE-computed, coupled and uncoupled plates; –·–, uncoupled plates, asymptotic modal density in equation (1). A total of four and two false (zero energy) modes are removed from the FE-computed uncoupled large and small plate eigenfrequency plots, respectively.

As a first analysis step, the FE computed modal count was examined to discover whether the FE computed modal count could help yield an improved estimate of the modal density. Modal density is a concept that is asymptotically derived from the modal count and, strictly speaking, is valid only when a large number of eigenmodes is included in the summation of the modal count [24, 25]. The asymptotic modal density, n_j, for a thin plate is [26]

$$n_j = (A_j/h_j)\sqrt{3\rho_j(1 - v_j^2)/Y_j}, \tag{1}$$

where the plate area is A_j, the plate thickness is h_j, Young's modulus is Y_j, the density is ρ_j and the Poisson ratio is v_j.

Figure 2 shows that the asymptotic modal densities in equation (1) can be used to produce reasonable estimates of the modal counts for the frequency range considered and that the FE and analytical eigenfrequencies compare. However, Bolt has cautioned in reference [24] that the asymptotic distribution of eigenfrequencies applies only at high frequency, and that this limitation should be investigated for acoustical problems "where the dimensions of the apparatus and enclosures are often of the same order of magnitude as the wavelengths". Therefore, as few modes are included in the actual modal count at low frequency, no significant improvement in computing the modal density, e.g., by frequency band averaging the modal counts for the local subsystems, is expected when using the FE- or analytically-derived modal counts. As a consequence, the concept of asymptotic modal density is believed to be about as accurate for the L-shaped plate as is feasible to expect when applied to the individual case.

As a second analysis step, the FE model was verified by comparison with measurements. Ninety modes with eigenfrequencies up to 1341 Hz are included and the Steady State Dynamics option in ABAQUS [27] was used for the response summations. The agreement between the FE-computed and measured mobilities in Figure 3 is similar to that for other positions. Also, the case examined was verified by comparisons with an analytical model. Rain-on-the-roof excitation is approximated in the FE model by uncorrelated forces acting at every node in the respective subsystems. Sixty-one modes were incorporated in the

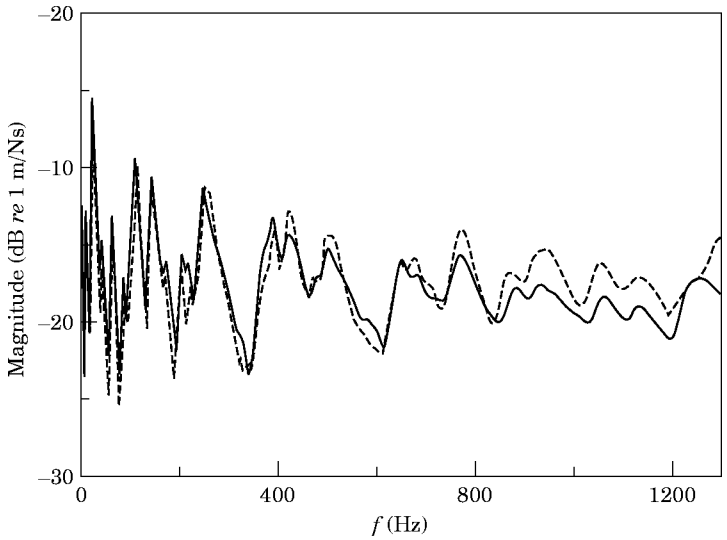

Figure 3. Magnitude of the driving point mobility at one of the free corners of the smaller plate: ——, measured; – –, FE computed.

response summation, with four modes outside the highest frequency 1300 Hz. The Random Response option in ABAQUS [27] was used to save computational time, as 651 separate computations with the Steady State Dynamics option would otherwise have been required to yield identical results. In the analytical model, modes with a free bending wavelength down to half the free bending wavelength at 1300 Hz were included in the response summation to reduce errors from modal truncation; i.e., modes with eigenfrequencies up to 5·2 kHz are included. Theory for the simple bending wave is applicable up to 10 kHz. Figure 4 shows the FE-computed and analytically derived kinetic energy for the case of simply supported boundaries and rain-on-the-roof excitation in the

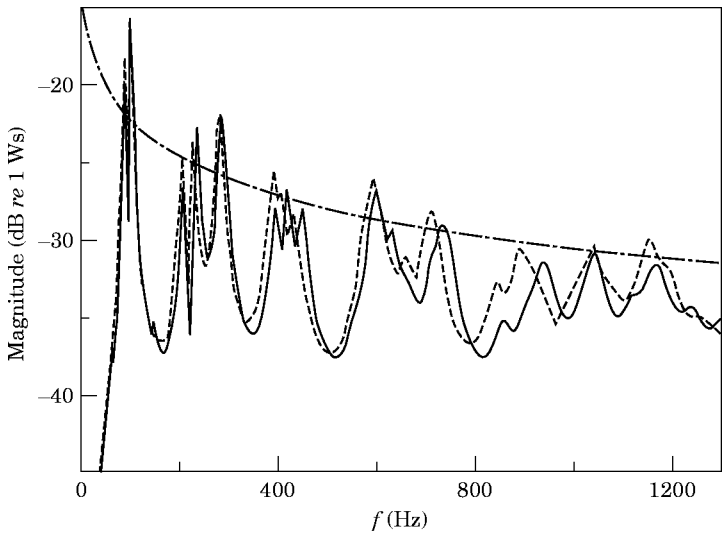

Figure 4. Kinetic energy for the smaller plate, $R_{11} \cdot S_1$: ——, analytical model; – –, FE computed; –·–, SEA-computed.

smaller plate. An example of the SEA-computed result is also included in the figure for comparison. The agreement for the case displayed is typical for that of other cases.

Figure 3 shows that the FE-computed mobilities are shifted downwards in frequency as compared with the experimental mobilities, with similar trends exhibited for the kinetic energies in Figure 4. This shift is likely to be caused by the reduced number of Gauss points in the finite elements (reduced integration) that may become overly weak [28]. Thus, the FE model is expected to produce a reasonable overall estimate of the vibrational behaviour for the L-shaped plate for various cases of boundary conditions and excitation, with good agreement at low frequencies and a downward trending shift at higher frequencies.

3. THE APPROACH

The energy flow is derived by combining an energy flow balance with FE computed data for the individual system. Note that a multitude of deterministic cases can be used to form an ensemble that, when sufficiently varied, provides the SEA ensemble's average coupling data. However, the individual case provides coupling data that typically differ from the mean value of the SEA ensemble, much in the same way that the election outcome of a community is not forecast by interviewing a single voter. This fundamental distinction between the individual and the ensemble should be considered in the derivation of coupling data and is stressed in the presentation below.

In this presentation, coupling data are derived in a way that in some aspects resembles procedures previously applied experimentally: e.g., the procedure in reference [29]. The term SEA-like is adopted to distinguish between SEA and the use of the energy flow balance for the individual case: i.e., to avoid confusing the statistic with the deterministic approach. Notations commonly used in SEA are applied in the energy flow model because of their familiarity and for convenience. Note that coefficients in the SEAL approach do not have exactly the same definitions as in SEA, even if they are used in a similar way. According to the distinction made in reference [30], the name Energy Flow Coefficient (EFC) is used when the deterministic approach is used and to distinguish it from the Coupling Loss Factor (CLF) as used in SEA. Similarly, the function necessary for energy flow reciprocity to exist is termed the reciprocity function in order not to confuse it with its SEA equivalent, the modal density ratio.

The individual case differs from what is predicted by SEA since its dynamic behaviour is influenced by features that are omitted in the SEA model: e.g., the distribution of natural frequencies, mode shapes etc. To identify such features, some assumptions in SEA should be considered; e.g.: (i) the non-resonant part of the subsystem energy that is provided by modes with eigenfrequencies outside the analysed frequency band is neglected; (ii) similarly, the total energy of a mode is assumed to be within the frequency band that is analyzed; (iii) the energy density should be constant over the subsystem; (iv) the source of excitation should be random in space and time and have a constant power spectral density; (v) the modal energies in the energy in the frequency band are considered to be incoherent to allow addition of their energy. Assumptions (i)–(v) are equivalent to replacing mode k's energy content, $2\Delta_e S_j M_k (M_k \omega_k \eta_k)^{-2}$, with the frequency spectral density for the modal energy, $2S_j M_k (M_k \omega_k \eta_k)^{-2}$, in the equivalent bandwidth, $\Delta_e = \pi f_k \eta_k / 2$, and assuming the subsystem energy to equal the energy provided by the (local) modes that lie within the frequency band [1]. The oscillator's physical mass is M_k, the damping η_k, eigenfrequency ω_k, and the power spectral density of the force amplitude is S_j. Figure 5(a) shows the response for a single mode and the mode's total energy that is within the equivalent bandwidth. The non-resonant part of the mode's energy that in reality falls outside the equivalent band, Δ_e, is often small when broad-band sources and frequency

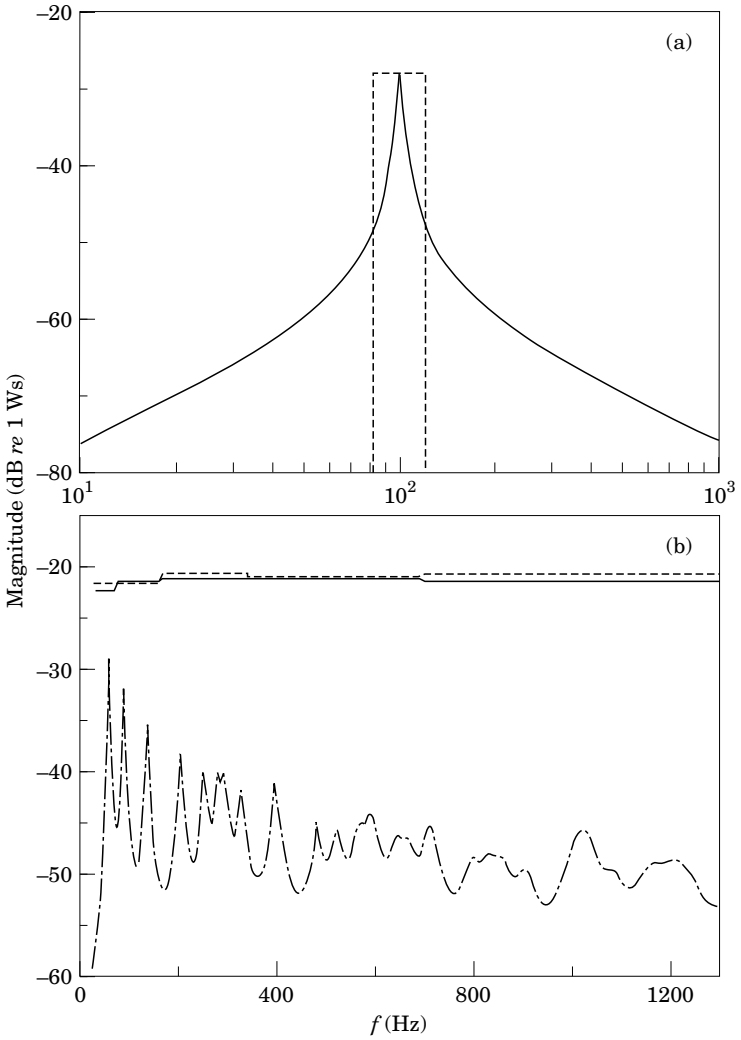

Figure 5. (a) The response of a single mode subjected to white random noise: ——, the frequency spectral density of the mode's kinetic energy; – –, the frequency spectral density of the modal energy in the equivalent band. (b) The response of a subsystem and the SEA realization for the frequency band: –·–, frequency spectral density of the deterministic subsystem response; ——, frequency band integrated deterministic subsystem response; —, subsystem response estimated by use of the (deterministic) modal count and the energy per mode.

bands containing several modes are considered. Its influence on the subsystem response can therefore often be suppressed when the two-subsystem case is examined. Figure 5(b) shows a case in which several modes are present. The frequency band integrated subsystem response is seen to be well described at most frequencies by the incoherent modal oscillators and the modal count. The dynamic features of the narrow band response, however are seen to be strongly influenced by non-resonant features at low frequency, although the non-resonant part of the subsystem energy contributes very little to the total energy of the frequency band. Therefore, there exist situations in which non-resonant features of a subsystem can dominate its dynamic behaviour, although the non-resonant part of the energy is barely noticeable for the frequency band. Examples of situations in which non-resonant features can dominate the dynamic behaviour are the following:

sources having a narrow band character; a non-uniform spectrum; forced excitation of systems with a low modal overlap. Another cause for deviation between the individual case and SEA is the assumption of spatially uncorrelated driving of uniform amplitude (rain-on-the-roof) which is biased if excitation acts at one or a few points. Therefore, when computing the response with conventional SEA, the degree of approximation for the individual case can be expected to depend on the type and magnitude of damping, the eigenfrequency separation, source position, the number of modes situated in the frequency band, and the source's frequency spectrum.

When accounted for in SEA, non-resonant transmission mechanisms are included in the power input or as conservative transmission paths in the power balance. Examples of these mechanisms are the well-known mass law for sound transmission between rooms, and exciting a structure through a stiff component attached to the structure. The former example includes non-resonant transmission between the rooms, and the latter case is treated as a power input that fits the non-resonant transmission characteristics in the stiff component. However, the non-resonant part of the kinetic energy is never explicitly used and thus the wall or stiff component cannot be regarded as a separate subsystem in SEA. A modal description of decaying fields require that many modes are included in the summation. Most of these modes do not have their natural frequency in the vicinity of the frequency of interest. Another example of a non-resonant transmission mechanism is therefore the near field that exists near the source and at the junction. When using FE-computed or measured data, where the non-resonant part of the kinetic energy is automatically included, a SEAL is formed where the non-resonant transmission mechanisms are directly incorporated. As a consequence, coupling data and the energy flow balance for the individual case should not necessarily be treated or interpreted in line with conventional SEA theory, in which such features are omitted.

Several procedures for determination of coupling data from the two subsystem configuration exist in the literature. An alternative approach that can be used for the individual case has been suggested in references [16, 17]. The subsystem energy and the energy flow can be described as a function of the excitation of amplitude S_j, as

$$\begin{Bmatrix} E_1 \\ E_2 \end{Bmatrix} = \begin{bmatrix} R_{11} & R_{12} \\ R_{21} & R_{22} \end{bmatrix} \begin{Bmatrix} S_1 \\ S_2 \end{Bmatrix}, \qquad \text{and} \qquad P_{1\to 2} = [P_{21} \quad P_{12}] \begin{Bmatrix} S_1 \\ S_2 \end{Bmatrix}, \tag{2, 3}$$

respectively. The vector $\{E_j\}$ and $P_{1\to 2}$, respectively, denote the subsystems' time average kinetic energy and time average active energy flow in the direction from subsystem 1 to subsystem 2. These are generated by the excitation S_j that is uncorrelated between subsystems i and j. The subsystem coefficients for the energy flow to subsystem i and the energy in subsystem i caused by the excitation in subsystem j are denoted P_{ij} and R_{ij}, respectively.

Combining equation (2) with equation (3) provides the energy flow balance for the two subsystem configurations:

$$P_{1\to 2} = [P_{21} \quad P_{12}] \begin{bmatrix} R_{11} & R_{12} \\ R_{21} & R_{22} \end{bmatrix}^{-1} \begin{Bmatrix} E_1 \\ E_2 \end{Bmatrix} = \omega [\eta_{12} \quad -\eta_{21}] \begin{Bmatrix} E_1 \\ E_2 \end{Bmatrix}, \tag{4}$$

where ω is the angular frequency and the matrix $[\eta]$ represents the EFCs.

It is noted that the above formulation for constructing energy flow models is automatic and places the couplings at the correct position in the matrix. It is observed as well that the number of co-ordinates necessary to describe the energy flow with the FE model has

been reduced, from 3816-degrees-of-freedom or 61 modes, to four co-ordinates. It should be noted, however, that in equation (4) the actual flow of energy and subsystem energy are used as input data to the energy flow balance when deriving the EFCs: i.e., the actual energy flows and responses must be known before the EFCs can be assessed. Thus, the EFCs are not necessary to predict the energy flow, ($P_{1\to 2}$), in the FE model unless it is sought from information about the total subsystem energies (E_1 and E_2) when excitations S_1 and S_2 act simultaneously in the subsystems. Therefore, the reasons for proceeding with the EFCs are the possibility of incorporating the deterministic model with a statistical one into a hybrid energy flow model for further processing, to yield data for configurations that are difficult to analyze by other means, and to judge at what frequency the deterministic approach can be shifted to a statistical one for gains in time- and cost-effectiveness. Furthermore, it can be noted that equation (4) is independent of requirements regarding the power spectral density for the excitations: i.e., it applies for narrow bands as well as for wider frequency bands and for sources located at one or a few positions. Using equation (4) for narrow bands allows the derivation of coupling data for steady state sources with any spectrum as long as the sources are independent between subsystems. Applying equation (4) for the wider frequency band requires the source's power spectral density to be constant in frequency.

The subsystem's kinetic energies are approximated as

$$E = \frac{\omega^2}{2} \sum_{k=1}^{N} m_k \hat{u}_k^2 \tag{5}$$

from the FE-computed data. The mass m_k and the nodal displacement $\hat{u}_k$ refer to node k in the FE model: i.e., the influence from the rotational degrees of freedom is assumed negligible.

The energy flow equals the power dissipated in the plates: i.e.,

$$P_{12} = \omega \eta_{d,1} R_{12} \approx 2\omega \zeta_1 R_{12} \qquad \text{and} \qquad P_{21} = \omega \eta_{d,2} R_{21} \approx 2\omega \zeta_2 R_{21}. \tag{6a, b}$$

The respective loss factors that relate to kinetic energy and the critical damping ratio in subsystem j are denoted $\eta_{d,j}$ and ζ_j.

The simplified loss factor in the RHS of equations (6a, b) is not necessary, in principle, as the dissipated power can be assessed from separate post-processing of the modal data; it is, however, justified from a practical point of view, as ABAQUS does not provide the dissipated power as output. No such assumptions are made in the analytical model and the explicit energy flow is used for comparison. Also, note that $\eta_{d,j}$, η_j and ζ_j have different definitions. The loss factor that relates to kinetic energy, $\eta_{d,j}$, is defined by equations (6a, b). The dissipation loss factor η_j, as used in SEA, has a similar definition and applies for a group of modes of equal amplitudes in a frequency band. The critical damping ratio, ζ_j, depends on the modal number. The loss factors, $\eta_{d,j}$, and ζ_j, relate to a good approximation to $\eta_{d,j} = 2\zeta_j$ at the eigenfrequencies. The dissipation loss factor, $\eta_j = 2\zeta_j$, applies for frequency bands in which the critical damping ratio is independent from the mode number. Figure 6 shows that the approximation in equations (6a, b) is reasonable at frequencies higher than the first (local) eigenfrequency in the subsystem. Further, the closest agreement between the actual and assumed loss factors in Figure 6 is, as expected, at the eigenfrequencies. The discrepancy between the loss factors increases with the distance in frequency from the closest (local) eigenfrequency. Thus, frequencies well below the first (local) eigenfrequency and cases with small modal overlap should be included in the analysis only if the dissipated power is explicitly evaluated.

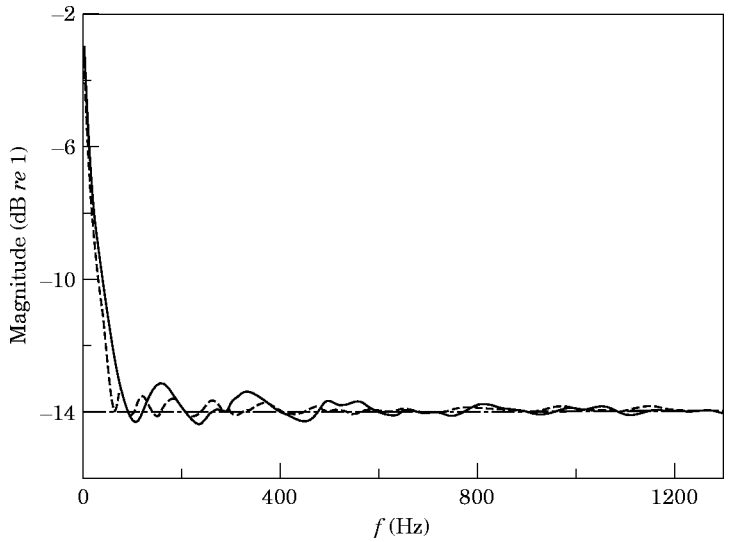

Figure 6. Loss factors referring to kinetic energy in equations (3a, b): ——, $\eta_{d,1}$, analytical model; – –, $\eta_{d,2}$, analytical model; –·–, $2\zeta_1$, the approximate loss factor.

4. RESULTS

4.1. ENERGY FLOW

The energy flow is obtained by using

$$P_{1\to 2} = \omega\eta_{12}E_2(E_1/E_2 - \eta_{21}/\eta_{12}). \tag{7}$$

Equation (7) yields the energy flow $P_{1\to 2}$ in Figure 7.

For clarity, the manner in which equation (7) is utilized for discrete frequencies and the single case is only SEA-like. A similar equation is normally applied for the frequency band in SEA when applied to the single case. Alternatively, the equation can be applied at a

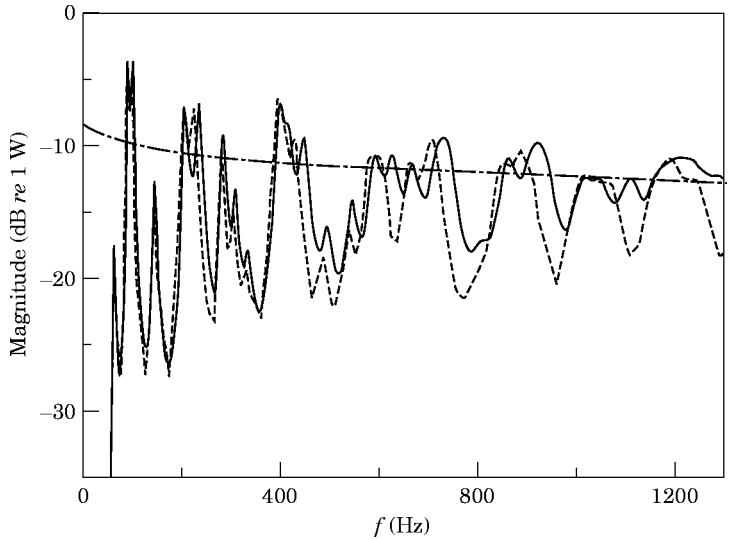

Figure 7. Energy flow, $P_{1\to 2}$, across the junction when exciting in the larger plate, equation (9): ——, analytical model; – –, FE-computed; –·–, SEA-computed.

discrete frequency for the SEA ensemble. The frequency band version is applied under the assumption that frequency band averaging is equivalent with ensemble averaging. Such assumptions are not made here, and thus the distinction of SEAL.

As expected, Figure 7 shows that energy flows from the excited subsystem to the receiver subsystem and demonstrates that a deterministic energy flow model can be used at any frequency. A good agreement exists between the FE- and analytically-derived energy flows, and it is concluded that the FE model, combined with a SEAL approach, yields a useful estimate for the power transmission between the two plates. The SEA-computed energy flow, as expected, is seen to be useful for the individual case at high frequency.

The variation in magnitude for the energy flow is reduced with increasing modal overlap [19, 20, 31]. The modal overlap is

$$M = f\eta_j n_j. \tag{8}$$

where f denotes frequency, η_j is the dissipation loss factor as used in SEA and n_j denotes the asymptotic modal density per Hz in subsystem j.

SEA, in its traditional form, is considered to provide results that diverge systematically and with an increased degree of uncertainty for frequencies at which the modal overlap is low [19, 20, 31]. For the case investigated, the modal overlap is unity at 1560 Hz for the smaller plate and at 780 Hz for the larger plate. The geometric mean of the subsystems' modal overlap [19] is unity at 1100 Hz. Therefore, SEA is expected to produce an estimate of the coupling data, responses and energy flow that improves in similarity to the examined case as the frequency increases.

4.2. ENERGY FLOW COEFFICIENTS AND ENERGY FLOW RECIPROCITY

The CLF is [26]

$$\eta_{ij} = c_{gi} L \tau_{ij} / \pi \omega A_i, \tag{9}$$

where c_{gi} is the group velocity for free bending waves in subsystem i, L is the junction length, A_i is the area of subsystem i and τ_{ij} is the transmission factor for transfer of power from subsystem i to subsystem j. The transmission factor 0·3 is used for all examples in this paper. The use of the transmission factor either for normal incidence (0·5) [26] or for diffuse incidence (0·3) [26] is felt to be rather arbitrary, as the incidence angle is neither normal nor diffuse and the weighting function for the incidence should not be uniform (diffuse) for the individual case. Furthermore, the above transmission factor accounts only for resonant transmission, something which may bias its estimate for the individual case. The negative values of the EFCs in Figure 8 clearly demonstrate that measured or computed results for the individual case should not be treated as, or interpreted in-line with conventional SEA theory.

The EFCs in Figure 8 tend, as expected, towards the CLF at high frequency and can be used to determine the case in which the approach can be changed from deterministic to SEA. A considerable deviation between the EFCs and the CLF is exhibited at low frequency, where the assumptions of free waves between resonance frequencies and uniform energy density in the subsystems become obscure. It is also observed that the EFC can be negative at some frequencies. A comparison between Figures 7 and 8 shows that the negative values for the EFC coincide with the largest peaks in the energy flow for the individual case. Therefore, the phenomenon that produces the negative values for the EFCs cannot be insignificant and motivates closer inspection. Note that negative EFCs, as opposed to negative CLFs in SEA, do not mean that energy flows in a direction towards its source or that the flow is of infinite magnitude. However, it does

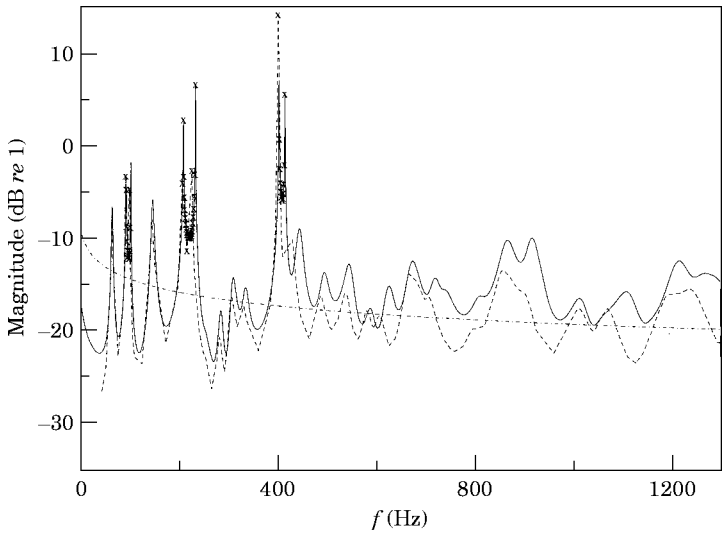

Figure 8. Coupling coefficients for the simply supported L-shaped plate, η_{12}: ——, EFC, analytical model; – –, EFC, FE-computed; –·–, CLF as used in SEA, equation (6); × ×, negative values.

imply that energy can flow from one subsystem with quite a small amount of kinetic energy density to another with a large amount of kinetic energy density.

Furthermore, one should be cautious about relying on analogies to the energy per uncoupled mode, as the current approach refers to coupled systems and, thus global modes. The correlation between an infinite number of uncoupled modes from both subsystems is required to represent a coupled mode. The concept energy per *uncoupled* mode case can be a poor descriptor when the case is strongly coupled and the response is clearly characterized by the shape of one or a few global (*coupled*) modes. The concept of uncorrelated *uncoupled* modes and the number of *uncoupled* modes can thus be a poor approximation of the *coupled* subsystem energy when coupling is strong.

In SEA, reciprocity for the flow of energy between two subsystems is

$$\eta_{12} n_1 = \eta_{21} n_2. \tag{10}$$

In the SEAL approach, the ratio between the EFCs defines the actual function for energy flow reciprocity, and explicit use of modal density is not made. Figure 9(a) shows that the reciprocity function tends towards the asymptotic modal density ratio at high frequency.

Figures 7, 8(b), 9(b), equations (2) and (9) reveal that the EFCs are negative when

$$R_{11}/R_{21} < \eta_{21}/\eta_{12} < R_{12}/R_{22} \tag{11a}$$

and ambiguously defined or of infinite magnitude when

$$R_{11}/R_{21} = R_{12}/R_{22} = \eta_{21}/\eta_{12}: \tag{11b}$$

i.e., when the $[R]$ matrix in equation (2) is singular. Combining equation (7) with equation (11b) shows that a coupling of infinite magnitude is multiplied with a difference of zero. Therefore, as is depicted in Figure 7, energy flows from the excited subsystem to the receiver subsystem when the EFCs are negative and at finite amplitude when the $[R]$ matrix is singular. In conventional SEA, equation (11b) would imply equipartition of modal energy and that the energy flow would be zero. This is clearly not the case, and again it is observed that the individual case differs from what applies from the SEA ensemble. The existence of flow of energy in the direction from low to high energy density has been

discussed by Mace in reference [32] where similar findings are shown to apply for the SEA ensemble, when the subsystem energy refers to the coupled system.

Equation (11a) has a kinetic energy that is larger in the receiving than in the excited subsystem. This indicates that transmission from the excitation positions through the excited subsystem is non-resonant when the EFCs are negative. In the two-subsystem case, non-resonant transmission occurs when the system is forced to respond at frequencies between well-separated (local) resonance frequencies of the excited subsystem. The excited subsystem behaves as a spring or mass at these frequencies and transmits power from the source to the joint. Figure 10(a) shows that the power input can be efficiently transmitted through the excited subsystem when the frequency is close to a (local) eigenfrequency of the receiving subsystem, as the excited subsystem is unable to accumulate more energy than the receiving subsystem at this frequency. The power dissipation in the excited subsystem is of course quite small when it is driven between well-separated eigenfrequencies: i.e., at

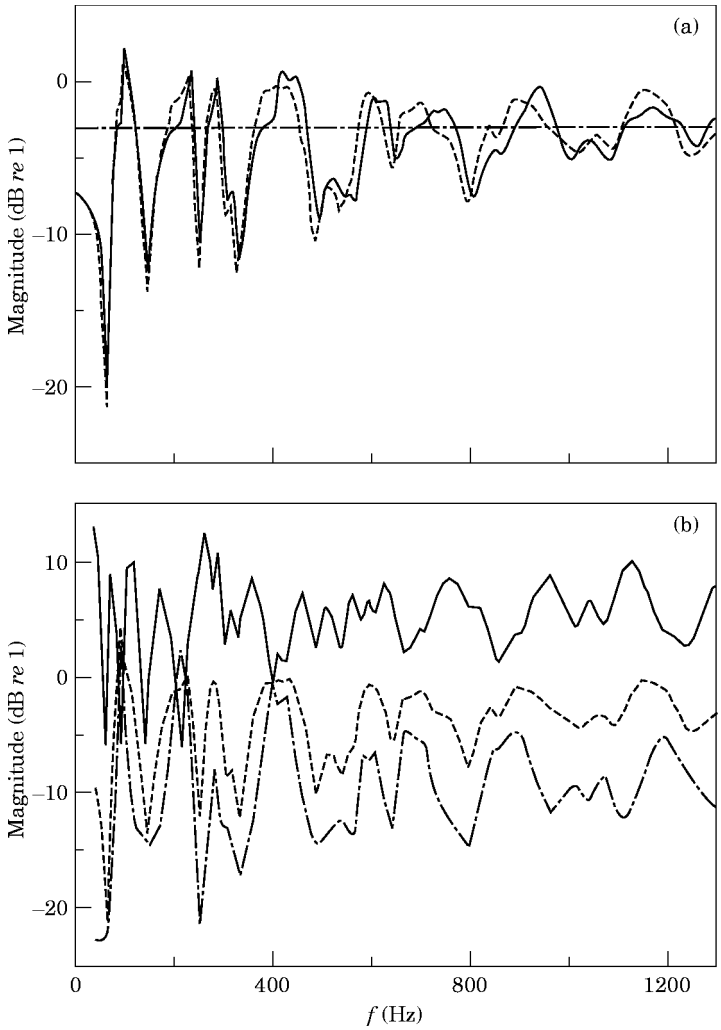

Figure 9. (a) Energy flow reciprocity function: ——, η_{21}/η_{12}, analytical model; – –, η_{21}/η_{12}, FE-computed; –·–, n_1/n_2, asymptotic modal density ratio, equation (1). (b) Conditions for negative EFCs or EFCs of infinite magnitude, equations 11(a, b): ——, kinetic energy ratio, R_{11}/R_{21}; –·–, kinetic energy ratio, R_{12}/R_{22}; – –, reciprocity function, η_{21}/η_{12}. FE-computed results.

frequencies where an anti-resonance occurs for the subsystem energy. Because the power that is transmitted from subsystem 1 to the receiving subsystem 2 is accounted for in this situation by the largest loss factor, η_{21}, and the largest subsystem energy, E_2, it is only natural the EFC should take on a negative value. This type of transmission path is not included in traditional SEA, and its influence is easily suppressed in the frequency band integrated subsystem response, but not in the EFC because it reflects upon the magnitude of the energy flow. The energy flow of the examined case is dominated by the above mentioned non-resonant transmission mechanism.

Figures 10(b–d) show a case in which this type of transmission mechanism is important. Figure 10(b) shows the two (local) mode shapes that have identical eigenfrequencies when the plates are not coupled along the common edge. The two (local) eigenfrequencies, (○ and *), split in frequency when the plates become coupled. One mode's eigenfrequency, (×), is shifted upwards in frequency as it becomes constrained by the other plate. The other mode remains at the original undamped eigenfrequency, (+), or is shifted upward in frequency when subjected to the constraint that is imposed by the other plate, reference

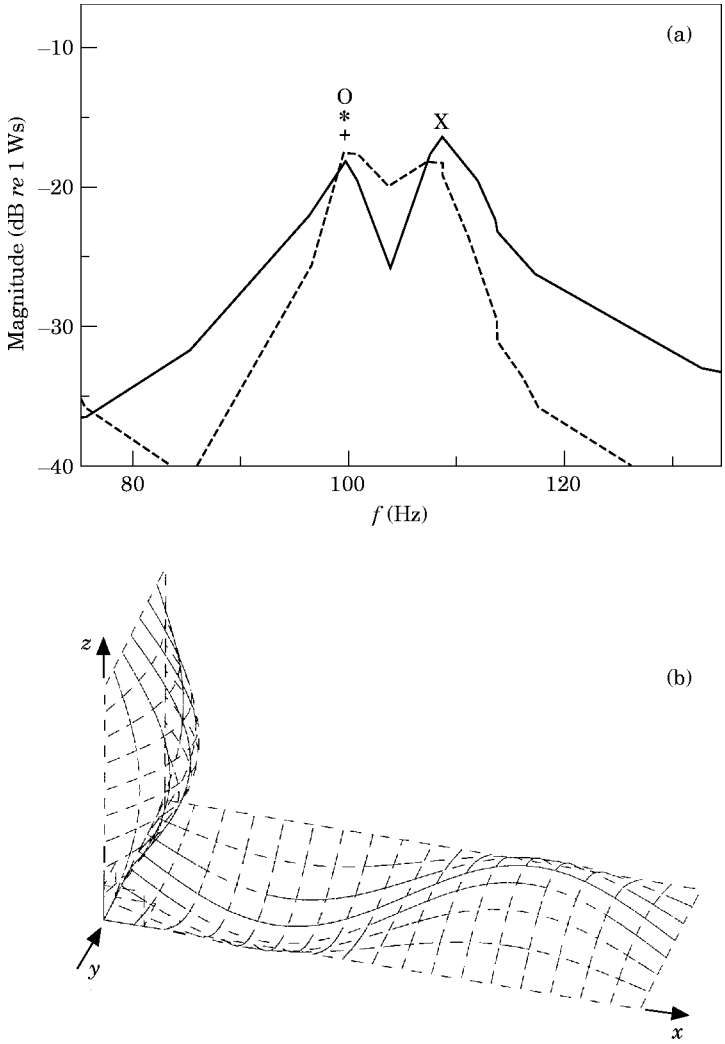

Figure 10 (a and b) *See caption opposite*

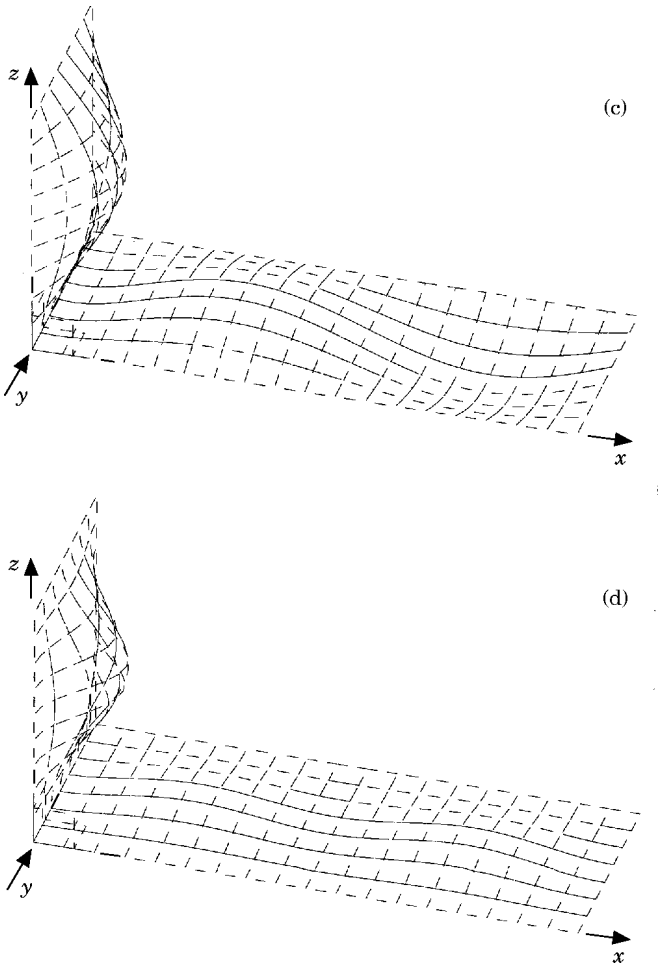

Figure 10 (c and d)

Figure 10. A case in which non-resonant excitation is important, FE-computed data. (a) The kinetic energy of the L-shaped plate: ——, the (larger) excited plate; – –, the (smaller) receiving plate. The eigenfrequencies: ○, (local) of the smaller plate when uncoupled; *, (local) of the larger plate when uncoupled; +, ×, (global) when the plates are coupled. (b) The (local) mode shapes when the plates are not coupled and one identical (global) mode shape for the coupled case, eigenfrequency *circa* 100 Hz. (c) A (global) mode shape for the coupled case, eigenfrequency *circa* 109 Hz. (d) The random response field when the larger plate is subjected to rain-on-the-roof excitation.

[33]. Figure 10(c) shows the (global) modeshape (×) that is shifted upwards in frequency. The other (global) modeshape (+) is identical to the (local) modeshapes (○ and *) in Figure 10(b), that remain at the original eigenfrequency when the plates are coupled along the common edge. The non-resonant behaviour of the larger plate is important when exciting in the larger plate, because energy can efficiently be transmitted to the receiving (smaller) plate where a (local) mode can absorb it. The global mode shapes in Figure 10(b, c) interfere and produce a response field in the larger plate that is quite small when it is subjected to rain-on-the-roof excitation. As depicted in Figure 10(d), energy flows from low to high energy density in this situation. It is observed that increasing the level of damping does not affect the shape of the (global) modes (of the mathematical model) in Figure 10(b, c) and, thus, the above mentioned phenomenon can also be expected to apply at high modal overlap. The above mentioned transmission mechanism cannot be included

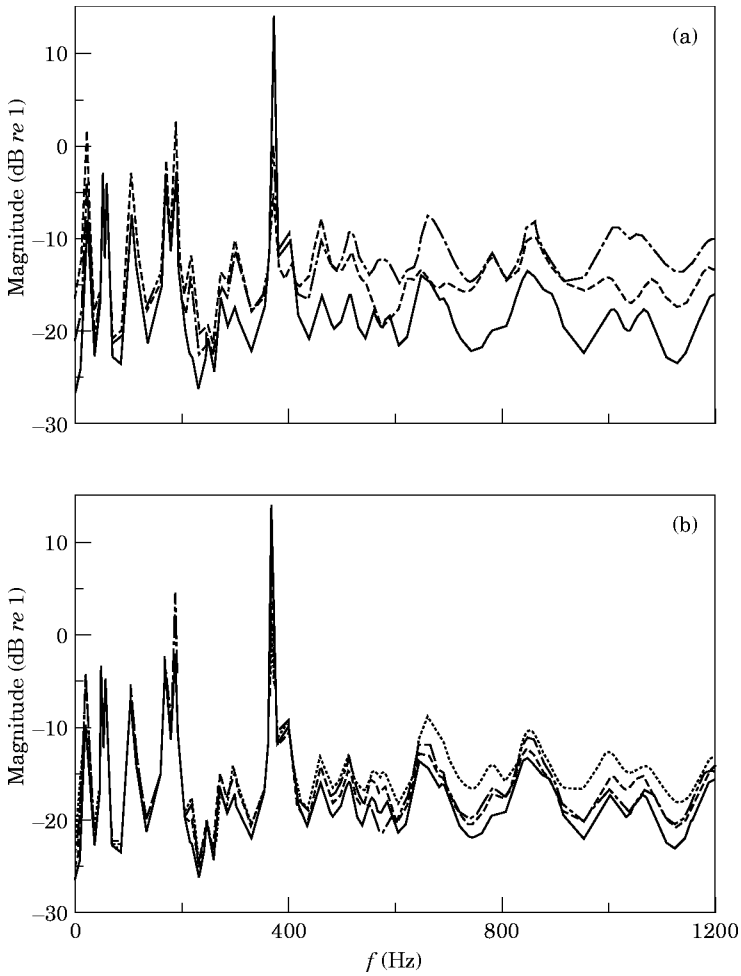

Figure 11. Variation of $|\eta_{12}|$ with excitation. (a) Different excitation positions: ——, rain-on-the-roof-excitation; – –, –·–, two sets with three excitation points per subsystem. (b) Different number of excitation points: ——, rain-on-the-roof-excitation; – –, 20; –·–, 10; · · ·, 6 excitation points per subsystem.

in SEA without excluding the assumption of modal incoherence, i.e., without utilizing some form of phase information in the SEA model.

The SEA model is reliable only for the individual case when the modal density ratio resembles the reciprocity function. Therefore, comparing the reciprocity function with the asymptotic modal density ratio in the SEA model seems to be a reasonable test limit for the transition from the deterministic energy flow approach to SEA, as was suggested for experimental work in reference [34]. Figure 9(a) shows that the asymptotic modal density ratio gives a reasonable estimate of the reciprocity function for frequencies at which the modal overlap is larger than unity. The reciprocity function, η_{21}/η_{12}, and the asymptotic modal density ratio, n_1/n_2, are observed to differ substantially at low frequency, in spite of the closeness between the actual and asymptotic modal counts in Figure 2. Therefore, assumptions that are valid in SEA should not be taken for granted without due consideration taken to their underlying assumptions when analyzing the individual case. Further, large fluctuations in the reciprocity function are exhibited at frequencies at which a low modal overlap occurs and, in particular, at frequencies at which non-resonant

transmission mechanisms are present. The above test forms an alternative to the modal overlap and seems to be useful as a test limit for the importance of non-resonant behaviour when combined with equations (11a, b) [35].

4.3. CHARACTERISTICS OF THE EFCS

Rain-on-the-roof excitation is sometimes assumed to approximate to a modest number of excitation points in each subsystem. Variations in the EFC estimates with excitation position are shown in Figures 11(a, b) and demonstrate that the EFC is not the same when different positions or a different number of points are used to excite the subsystems. The results tend, as expected, towards the case of rain-on-the-roof excitation with an increasing number of excitation points. Also, the EFCs in Figures 11(a, b) can be observed to be biased in magnitude when a different number of excitation points are used. This bias

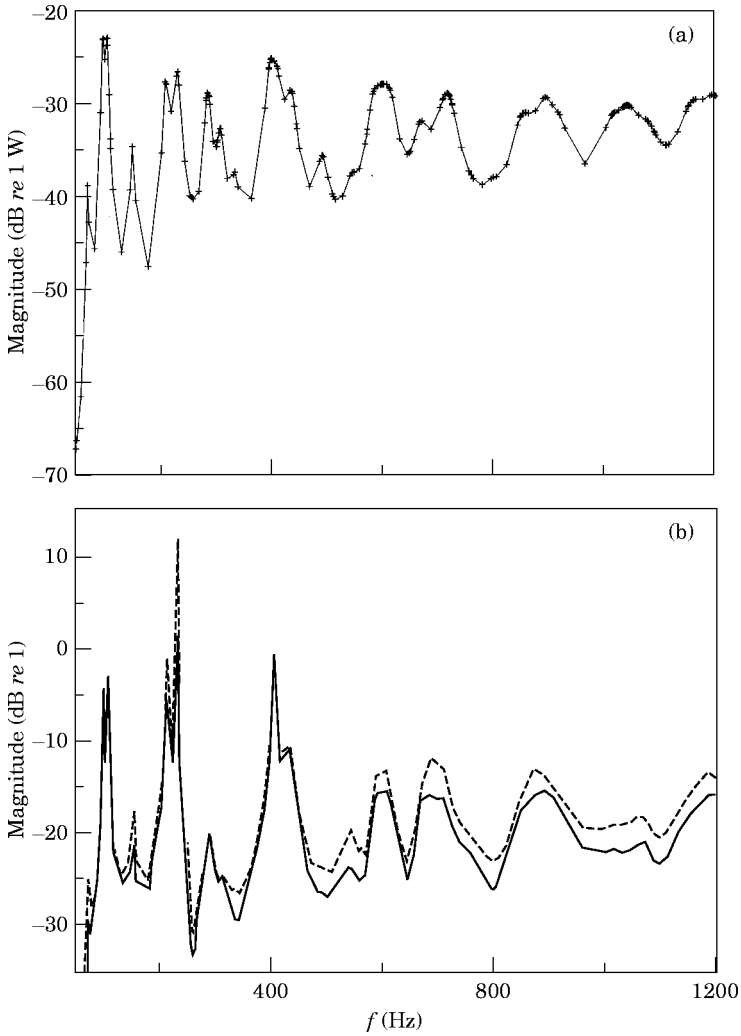

Figure 12. The energy flow from a source in subsystem 1. (a) Energy flow across the joint, $P_{1\to2}$: ——, rain-on-the-roof; + + +, three points. (b) The EFC, $|\eta_{12}|$, from the two sets of excitation positions. Number of excitation positions in the receiving subsystem 2: ——, rain-on-the-roof; – –, 3 points.

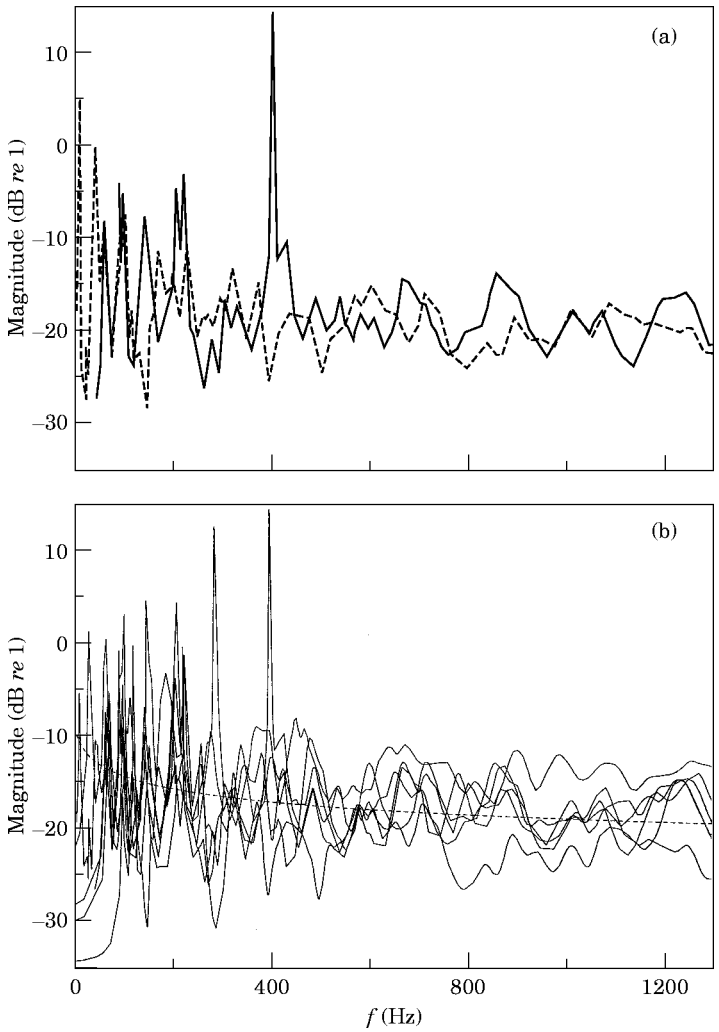

Figure 13. (a) Variation in $|\eta_{12}|$ with boundary conditions, rain-on-the-roof excitation: ——, all sides simply supported; —, simply supported joint and the other sides free-free. (b) Variations in $|\eta_{12}|$ with shape for six cases with identical subsystem sizes of varying shape.

depends on the number of excitation positions that generate the subsystem coefficients in equations (2) and (3).

Deviation between EFCs referring to a particular excitation or rain-on-the-roof excitation does not imply that any of the derived EFCs are less valuable or more valid than others, but simply that they apply for different cases. Thus, the energy flow for rain-on-the-roof excitation is not predicted with EFCs from another case and, by analogy, the energy flow for a particular source is not necessarily well described by the EFCs from rain-on-the-roof excitation. As an example of the above, it is equally good to excite at a single point as to excite with rain-on-the-roof excitation in the receiver subsystem when gathering data to solve equation (4) and the (source) excitation of interest occurs in one subsystem only. The energy flow from the source subsystem to the receiving subsystem is naturally the same regardless of the excitation in the receiving subsystem, as long as the source and the other excitation are independent. Figure 12(a, b) confirms that the identical

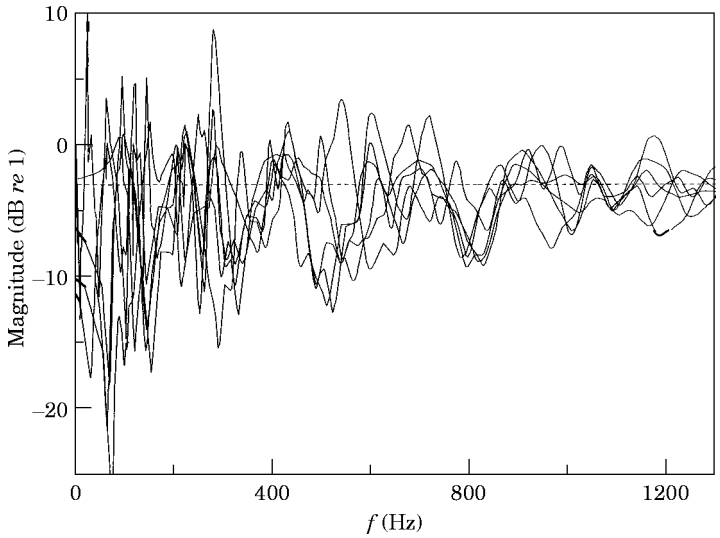

Figure 14. Variation in the reciprocity function for the cases in Figure 13(b). ——, FE-computed; – –, SEA values.

energy flow, $P_{1\to2}$, is assessed for the identical source when using EFCs derived from two different sets of excitation points in the receiving plate, and that this transmission is represented by two different sets of EFCs.

The EFCs, as opposed to the CLFs in SEA, are influenced by the subsystems' shapes and boundary conditions, which is confirmed in Figure 13(a, b), where the EFCs from two cases of boundary conditions and various subsystem shapes are compared. The subsystems are varied such that their respective area is constant and the distortion of the FE mesh for skew, taper and aspect ratio is within the limits specified in reference [22]. A characteristic trend that is similar to the CLF can be seen for the EFCs displayed at high

TABLE 1

The table can be interpreted as follows. Statistical Energy Analysis is a statistical approach that applies to ensembles and uses the Coupling Loss Factor to describe the flow of energy between parts. SEA is applied at "high" frequency, uses concepts that are invariant to geometry, etc., excludes explicit use of the non-resonant part of the subsystem energy and, thus, normally excludes non-resonant transmission mechanisms. The SEAL approach is deterministic, applies for the individual case and uses the Energy Flow Coefficient to describe the flow of energy between parts. The SEAL approach is applicable at any frequency, uses concepts that vary with geometry, etc., allows explicit use of the non-resonant part of the subsystem energy and thus, automatically includes non-resonant transmission mechanisms

SEA	SEAL
A statistical approach	A deterministic approach
Ensembles	The individual case
Coupling Loss Factor (CLF)	Energy Flow Coefficient (EFC)
"High" frequency	Any frequency
Invariant to geometry, etc.	Varies with geometry, etc.
Normally excludes non-resonant transmission mechanisms	Includes non-resonant transmission mechanisms

frequency, although their behaviour is quite individual at low frequency. Two graphs in Figure 13(b) have values at high frequency that are shifted in magnitude relative to the other EFCs. These graphs refer to cases in which the subsystems have a tapered shape. The junction length is changed with respect to the other cases for the tapered configurations and, thus, the EFC is shifted upwards in magnitude for the longer and downwards in magnitude for the shorter joint. Figure 14 shows the variation in reciprocity function for the cases of Figure 13(b) where, again, a characteristic trend is observed at high frequency with the individual behaviour at low frequency.

In summary, a list of aspects that differ between the statistical and deterministic energy flow balances is shown in Table 1.

5. CONCLUSIONS

The possibility of combining the Finite Element method with an energy flow balance for derivation of energy flow within a system has been demonstrated. A commercial Finite Element code was used to derive the energy flow and its associated Energy Flow Coefficients. Advantages of this approach are found in its versatility in dealing with complicated subsystem topologies, complicated joints, sources with frequency spectra containing narrow bands, non-resonant transmission mechanisms, the small number of co-ordinates describing the energy flow and the simplicity in dealing with scalar quantities. Application of a SEAL approach is suggested as a complement to existing methods for the generation of input data for sections at which traditional SEA provides a poor estimate. In addition, the SEAL approach can be used as a tool for testing the suitability of conventional SEA for the individual case.

Use of this technique for the assessment of energy flow within a thin L-shaped plate was compared with results from an analytical model. The inclusion of information concerning the non-resonant behaviour in the energy flow model was shown to increase the applicable frequency range to frequencies below the first eigenfrequency. Furthermore, it is concluded that EFCs, as opposed to the CLFs in SEA, are case specific: i.e., dependent on the system properties, boundary conditions and excitation. The existence of negative EFCs was exemplified and demonstrated to occur when non-resonant transmission from the source through the excited subsystem was substantial. Consequently, the classical heat analogy is considered not to be applicable for direct interpretation of EFCs at frequencies at which a low modal overlap exists.

Familiar results were obtained confirming the high frequency tendency of EFCs and the reciprocity function to go towards the CLF and the asymptotic modal density ratio, respectively. For SEA to work properly for the single case, the SEA reciprocity relationship must resemble the derived reciprocity function reasonably well. Thus, it seems to be possible to use a comparison of the asymptotic modal density ratio with the reciprocity function as a test limit for the transition from the deterministic energy flow approach to SEA. This test can represent an alternative to the modal overlap as a test limit for the importance of non-resonant transmission and the non-resonant part of the subsystem's energy in the energy flow balance.

ACKNOWLEDGMENTS

The author gratefully acknowledges the support received from the Swedish Board for Technological Development (NUTEK), the Swedish Work Environment Fund (AMFO) and the Swedish Building Research Council (BFR). He also would like to thank Professor Tor Kihlman for encouragement and guidance throughout this project and the referees

for helpful comments on the paper. The author is grateful to Professor Juha Plunt for pointing out the significance of the first letter in "SEA".

REFERENCES

1. R. H. Lyon 1974 *Statistical Energy Analysis of Dynamical Systems—Theory and Applications*, Cambridge MA: M.I.T. Press.
2. A. S. Nikiforov 1979 *Vibration Absorption in Ships*. Leningrad: 'Sudostroenie' Publishing House. (In Russian).
3. T. Kihlman 1967 *Report from Byggforskningen*, *Stockholm* 9/67, Transmission of structure-borne sound in buildings.
4. L. E. Buvailo and A. E. Ionov 1980 *Soviet Physics Acoustics* **26**, 277–279. Application of the finite element method to the investigation of the vibroacoustical characteristics of structures at high audio frequencies.
5. D. J. Nefske and S. H. Sung 1989 *ASME Journal of Vibration Acoustics Stress and Reliability in Design* **111**, 94–100. Power flow finite element analysis of dynamic systems: Basic theory and application to beams.
6. O. M. Bouthier and R. J. Bernard 1992 *AIAA Journal* **30**, 616–621. Models of space-averaged energetics of plates.
7. P. C. Wood 1990 *Proceedings of the Institute of Acoustics* **12**, 571–578. The use of finite element methods in SEA application.
8. K. De Langhe, P. Sas and D. Vanderpitte 1994 *Proceedings of ISMA* 19, *Leuven*, *Belgium*, 471–480. Numerical simulation of waves in beams by using the finite element method.
9. J. M. Cuschieri 1990 *Journal of the Acoustical Society of America* **87**, 1159–1165. Structural power flow analysis using a mobility approach of an L-shaped plate.
10. L. Gavric and G. Pavic 1993 *Journal of Sound and Vibration* **164**, 29–43. A finite element method for computation of structural intensity by the normal mode approach.
11. S. A. Hambric 1990 *ASME Journal of Vibration and Acoustics* **112**, 542–549. Power flow and mechanical intensity calculation in structural finite element analysis.
12. C. R. Fredö 1993 *F* 93-01, *Licentiate of Engineering Thesis*, *Chalmers University of Technology*. Derivation of energy flow with a finite element model.
13. J. A. Steel and R. J. M. Craik 1994 *Journal of Sound and Vibration* **178**, 553–561. Statistical energy analysis of structure-borne sound transmission by finite element methods.
14. G. Stimpson and N. Lalor 1992 *Proceedings of Inter-Noise* 92, *Toronto*, *Canada*, 557–560. SEA extension of an FE model to predict total engine noise.
15. P. J. Remington and J. E. Manning 1975 *Journal of the Acoustical Society of America* **57**, 374–379. Comparison of statistical energy analysis power flow predictions with an "exact" calculation.
16. E. K. Dimitriadis and A. D. Pierce 1988 *Journal of Sound and Vibration* **123**, 397–412. Analytical solution for the power exchange between strongly coupled plates under random excitation: a test of statistical energy analysis concepts.
17. C. R. Fredö *Journal of Sound and Vibration* (to be published). Comment on: "Analytical solution for the power exchange between strongly coupled plates under random excitation: A test of statistical energy analysis concepts".
18. A. J. Keane and W. G. Price 1987 *Journal of Sound and Vibration* **117**, 363–386. Statistical energy analysis of strongly coupled systems.
19. F. J. Fahy and A. D. Mohammad 1992 *Journal of Sound and Vibration* **158**, 45–67. A study of uncertainty in applications of SEA to coupled beam and plate systems, Part 1: computational experiments.
20. B. R. Mace 1993 *Journal of Sound and Vibration* **166**, 429–461. Statistical energy analysis of two continuous one-dimensional subsystems.
21. C. Simmons 1991 *Journal of Sound and Vibration* **144**, 215–228. Structure-borne sound transmission through plate junctions and estimates of SEA coupling loss factors using the finite element method.
22. W. K. Borthwick and A. K. Ng 1989 *Proceedings of The Second International Conference on Quality Assurance in Finite Element Analysis*, 410–433. The influence of element shape on the dynamic analysis of flat plate structures.

23. I. A. ANDERSON 1990 8*th International Modal Analysis Conference*. *Kissimmee*, *Florida*, 673–678. Avoiding stinger rod resonance effects on small structures.
24. R. H. BOLT 1939 *Journal of the Acoustical Society of America* **10**, 228–234. Frequency distribution of eigentones in a three-dimensional continuum.
25. D.-Y. MAA 1939 *Journal of the Acoustical Society of America* **10**, 235–238. Distribution of eigentones in a rectangular chamber at low frequency.
26. L. CREMER, M. HECKL and E. E. UNGAR 1973 *Structure-Borne Sound*. Berlin: Springer-Verlag. See p. 453.
27. ABAQUS *V*. 4.9 *Theory and User's Manual*, Hibbit Karlsson & Sorensen, Inc.
28. NAFEMS 1991 *A Finite Element Primer*, 2*nd reprint*. Glasgow. NAFEMS Publications.
29. G. STIMPSON and N. LALOR 1990 *Proceedings of the Institute of Acoustics* **12**, 563–570. Using energy flow analysis techniques for the prediction of structural noise radiation.
30. R. H. LYON and T. D. SCHARTON 1965 *Journal of the Acoustical Society of America* **38**, 253–261. Vibrational energy transmission in a three element structure.
31. H. G. DAVIES and M. A. WAHAB 1981 *Journal of Sound and Vibration* **77**, 311–321. Ensemble averages of power flow in randomly coupled beams.
32. B. R. MACE 1994 *Journal of Sound and Vibration* **178**, 95–112. On the statistical energy analysis hypothesis of coupling power proportionality and some implications for its failure.
33. E. H. DOWELL 1979 *ASME Journal of Applied Mechanics* **46**, 206–209. On some general properties of combined dynamical systems.
34. J. S. POLLARD 1990 *Proceedings of Inter-Noise* 90, *Gothenburg*, *Sweden*, 953–956. Measurement of cylinder/plate coupling loss factors and associated problems.
35. C. R. FREDÖ and M. A. SANDERSON 1993 *Proceedings of Inter-Noise* 93, *Leuven*, *Belgium*, 1193–1196. Energy flow in an L-shaped plate.